

ORIGINAL ARTICLE

Elastic properties of multi-layered ceramic systems for SOCs

Alessia Masini¹  | Filip Šiška¹ | Oldřich Ševeček² | Zdeněk Chlup¹ | Ivo Dlouhý¹

¹Institute of Physics of Materials, AS CR, Brno, Czech Republic

²Faculty of Mechanical Engineering, Brno University of Technology, Brno, Czech Republic

Correspondence

Alessia Masini
Email: masini@ipm.cz

Funding information

CoACH – Advanced glasses, Composites And Ceramics for High growth Industries European Training Network (ETN), Grant/Award Number: 642557; GrInHy – Green Industrial Hydrogen, Grant/Award Number: 700300

Abstract

SOCs (Solid Oxide Cells) operate in harsh conditions and have to withstand considerable static and cyclic stresses, both mechanical and thermal. Thus, their mechanical stability is threatened. One fundamental aspect is the structural integrity of the cell. In fact, mechanical failure of a single cell can damage the whole stack, reducing the lifetime and the efficiency of the entire system.

This study focuses on the ceramic layered structure of an Yttria-stabilized electrolyte supported cell. Its elastic modulus has been measured through destructive and nondestructive techniques (three-point bending test, impulse excitation technique, tensile test). Many literature sources deal with properties of the most common electrolytes and electrodes, yet co-sintering effects and interactions between layers are still not fully comprehended. In this contribution the overall elastic performance of the cell has been investigated, focusing on the role that the interface between layers plays in the changing of resulting mechanical properties. To enable this investigation, layers were added to the electrolyte one by one, thus allowing individual interactions to be distinguished with the help of numerical simulations. Results obtained for consecutive samples through different techniques have been compared and discussed.

KEYWORDS

elastic constants, finite element analysis, fuel cells, layered ceramics

1 | INTRODUCTION

Saving fossil fuels and decreasing carbon dioxide emissions are two of the biggest challenges the energy market is facing nowadays; therefore, more environmentally friendly and efficient means of energy conversion are needed.¹ Solid Oxide Fuel Cells (SOFCs) and Solid Oxide Electrolyser Cells (SOECs) are clean and efficient technologies that promise to revolutionize the production of electricity and synthetic fuels²⁻⁴; however, their reliability has to be improved. Over the last decades, many efforts have been devoted to optimize stack design in order to improve system efficiency and lower the risk of degradation.⁵⁻⁷ Thermo-mechanical models have been increasingly used to simulate operational conditions, while trying to identify the magnitude of stresses arising in the whole stack as well as in the cell and that

might be responsible for failure.⁸⁻¹² This approach requires reliable values of the thermal and mechanical properties (e.g., elastic constants) of the materials involved.

Our work is currently focusing on the ceramic cell (also known as MEA, i.e., Membrane Electrolyte Assembly), as it is the core of a SOC stack and the understanding of its behavior is crucial for both the design and operation of the device. As a matter of fact, failure of a cell will be detrimental to the efficiency and the lifetime of the whole stack; hence the need to focus on mechanical performances of SOCs, besides electrochemical.¹³ The cell is a multilayered structure mainly consisting of two porous electrodes bonded to a dense electrolyte. In the last decades, many studies have been dedicated to the most common electrolyte and electrodes materials, yet mainly as individual layers or in their bulk form.¹⁴⁻²¹ Selçuk and Atkinson^{14,15} investigated the effective Young's

modulus and Poisson’s ratio of some materials of interest for SOFC, such as CGO, TZP, YSZ, and Ni-YSZ. Giraud and Canel¹⁶ continued the research on the elastic behavior of several materials commonly used in SOFC technology (YSZ, LSM, and Ni-YSZ). Kushi et al^{17,18} focused their studies on the measurement of elastic modulus and internal friction of conventional electrolyte materials. Other results on the mechanical characterization of SOC materials can be found in ref.^{20,21} As previously mentioned, all these studies evaluated electrolyte and electrode materials individually; the interactions between them, once they are co-sintered to take part in the cell structure, are still not fully understood. To obtain an accurate FEM model, it is necessary to gain knowledge on the behavior of material properties while exposed to service conditions. While the experimental assessment of the properties of electrolytes is quite easy, the same cannot be said about the electrode materials. This is due to the fact that electrodes are usually thin layers printed on a thicker electrolyte support and besides that, they are highly porous, with microstructure and mechanical properties strongly depending on the manufacturing process.²² Those are the reasons why mechanical properties of SOC materials are not fully understood and they have been mainly investigated through dense and porous thick specimens.²³ Even if nowadays numerical simulations become a useful tool to evaluate effective properties of real materials and to link the microstructure to the macroscopic properties, few studies have been performed to determine effective mechanical properties.^{24,25} The goal of the present contribution is to fill this gap, investigating the elastic behavior of the cell as an assembly. The influence that the interface between layers has in the changing of resulting elastic properties has been taken into account. To do so, destructive and nondestructive methods have been used. All experiments have been supported by numerical simulations because the standard evaluation of experimental data is usually limited to monolithic materials only and is not fully valid for thin multi-layered materials.

2 | EXPERIMENTAL PROCEDURE

Considering that the cell (MEA) is made up of co-sintered layers, the constraints arising between them will affect its overall properties. In order to understand the influence of each layer on the resulting Young’s modulus of the cell,

tests were carried out on samples with an increasing number of layers. Starting from the bare 3YSZ (Yttria-stabilized Zirconia) electrolyte, subsequent layers were added one by one: first the GDC (Gadolinium Doped Ceria) barrier layer, then the Ni-based fuel electrode and finally the LSCF (Lanthanum Strontium Cobalt Ferrite) air electrode. Tests were performed after every layer deposition. To easily identify the composition of samples, they were labeled as shown in Table 1.

2.1 | Samples preparation

All the materials tested were in as received state, i.e., as sintered and without any surface treatment. Specimens were extracted directly from SOC0 – SOC3 as-sintered plates of dimensions 100 mm × 150 mm according to Table 1. Two types of specimens were prepared:

1. Rectangular bars: cut by precision diamond saw Isomet 5000 (Buehler, Lake Bluff, IL), and carefully ground/polished edges afterwards, suitable for both flexural and resonance tests. In the first case the bars had dimensions of 7 mm × 25 mm x total thickness (see Table 1); while for the resonance test smaller bars of 5 mm × 13 mm x total thickness were prepared.
2. Dog-bone shaped bars: prepared by laser beam cutting, suitable for uniaxial tensile tests. No consequent edge treatment was applied. The samples had a total length of 88.5 mm and a gauge 42 mm long and 3 mm wide. Their geometry is illustrated in detail in Figure 1.

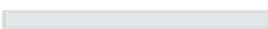
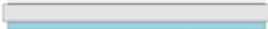
2.2 | Characterization

To characterize the elastic properties of the individual layers, three types of tests were performed using an impulse excitation technique (IET), flexural (3PB) and tensile (TENSILE) loading.

2.3 | Impulse excitation technique

Rectangular bars were tested using a IET equipment HT1600 (IMCE, NV, Genk, Belgium). The impulse excitation technique is a nondestructive method that provides fast, precise and repeatable measurements, therefore widely approved by science and industry.^{14,16,26-29} Flexural elastic

TABLE 1 List of the tested samples with a brief description, total nominal thicknesses (t_{tot}), and thickness of each added layer (t_{add})

Material	Schematic representation	Layers description	t_{tot} [μm]	t_{add} [μm]
SOC0		Electrolyte	94	–
SOC1		Electrolyte + GDC	101	7
SOC2		Electrolyte + GDC + fuel Electrode	125	24
SOC3		Electrolyte + GDC + fuel Electrode + air Electrode	174	49

(Young's) and shear moduli were calculated from the resulting first natural flexural and torsional resonance frequencies (eigenfrequencies), the sample density and dimensions according to the ASTM standard.³⁰ Poisson ratio was consequently determined using both flexural and torsional eigenfrequencies. Tests were carried out at room temperature and an isotropic elasticity was assumed for the evaluations, even though this condition was valid only for the electrolyte (SOC0). Even if we cannot speak about Elastic modulus in its physical meaning, this assumption allowed estimating the effective response of the laminates under investigation. To avoid undesired geometric effects, in-plane dimensions of the samples were kept unaltered for all layers combinations. The statistical data for each sample, plotted in Table 3, were determined from at least 20 independent measurements of the natural eigenfrequencies. The standard deviation of the measured frequencies was small. On the other hand though, the global uncertainty given by the precision of the measurement of weight and dimensions of the samples was relatively high (i.e., $\Delta E = 8.25$ GPa for SOC0 and $\Delta E = 1.04$ GPa for SOC3). This highlights how the thickness is the biggest source of error.

2.4 | Flexural test

The flexural elastic modulus was determined through flexural tests as well. Test rollers of 5 mm diameter with a 16 mm span were chosen for the three-point bend configuration. The measurements were performed in accordance to the standard EN 843-2³¹ in air at room temperature on rectangular bars with nominal dimensions of 7 mm \times 25 mm \times total thickness (see Table 1). The tests were carried out under displacement control using a universal test system Instron 8862 (Instron, Norwood, MA) with a 5 kN load cell; the cross-head speed was set to 1 mm/min. The deflection was measured by precise LVDT (HBM, Darmstadt, Germany) with a gauge length of 2 mm directly on the sample and verified by DIC (Digital Image Correlation) method.³² Since the aim was to determine the elastic modulus, samples underwent three loading-unloading cycles controlled by the total deflection of 1 mm. A typical load



FIGURE 1 Optimized geometry and dimensions (in mm) of tensile samples

versus displacement curve is illustrated in Figure 2. Both sides of each sample were tested (i.e., exposed to the tension) to evaluate the effect of the nonsymmetric layout of layers during bending. The flexural elastic moduli were calculated from the linear part of the unloading curve (see Figure 2), using the equation provided by the EN 843-2 standard:

$$E = \frac{al^3}{4bt^3} \quad (1)$$

where E is Young's modulus [MPa]; a is the slope of the unloading curve [N/mm]; b is the width of the specimen [mm], l is the span [mm], and t is the thickness of the specimen [mm]. The usage of the unloading part of the cycle was induced by the necessity of eliminating the friction effects caused by the extensometer and the rollers on the resulting modulus.

2.5 | Tensile test

Optimized dog-bone shaped specimens³³ were tested using the same Instron 8862 machine used for the flexural test with a 5 kN load cell and the crosshead speed of 100 $\mu\text{m}/\text{min}$. The samples had a gauge length of 42 mm; their geometry and dimensions are shown in detail in Figure 1. To ensure perfect grip between the fixture and the sample, sand paper was glued to the samples heads. Elastic properties were calculated from the force-displacement/elongations traces. The sample deformation was measured by DIC method.³² Digital images were recorded during the tests by a CCD camera EOS D40 (Canon, Tokyo, Japan) with an ultrasonic EF 100 mm f/2.8 Macro USM objective (Canon) positioned in front of the samples. Young's

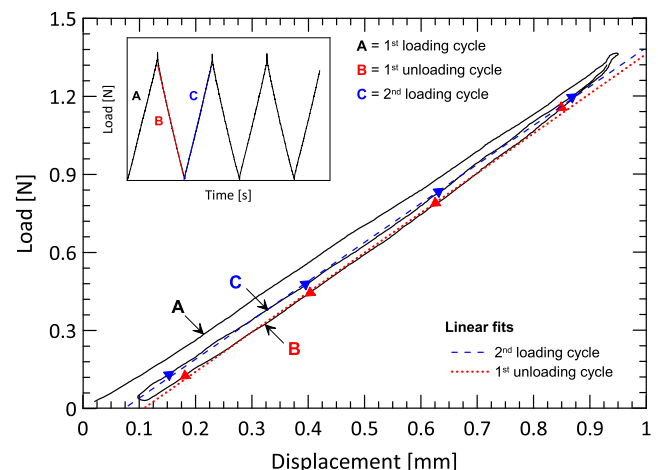


FIGURE 2 Typical load-vs-displacement curve, used for the evaluation of the E modulus from 3PB test

moduli were estimated according to the Hook's law from the calculated stress-strain curves.

2.6 | Analytical and numerical calculations

The IET and 3PB tests were supported by Finite Element Analysis (FEA) since the layered structure of specimens, being nonisotropic, invalidates standard approaches. Regarding the tensile test, FE simulations were not necessary, as the loading configuration allows the direct application of the rule of mixture (RoM). Starting from the data obtained through the tensile test, Young's modulus E_{add} of each added layer of thickness t_{add} was computed according to the rule of mixture from the apparent Young's modulus E_{app} determined experimentally of the whole laminate of thickness h (having totally n different layers) as follows:

$$E_{app} = \frac{E_{add} \cdot t_{add}}{h} + \sum_{i=1}^{n-1} \frac{E_i \cdot t_i}{h} \quad (2)$$

$$E_{add} = \frac{1}{t_{add}} \left(h \cdot E_{app} - \sum_{i=1}^{n-1} E_i \cdot t_i \right)$$

E_i and t_i are Young's modulus and thicknesses of already known layers in the multilayer structure, respectively.

2.7 | FE simulation of IET

Analogously to the experimental approach, but this time with the aid of FEA, the elastic moduli of individual layers were extracted from the results obtained by IET tests. The simulations were carried out stepwise for specimens SOC0-

SOC3. The general procedure of FEA employed is schematically represented in Figure 3. The iterative approach was applied to estimate properties of the added layer with set precision (step) ΔE meeting the experimentally determined eigenfrequencies for the whole sample. This semi-automatic approach, aided by the software Mathematica, is not able to distinguish nonsymmetrical layout and is working with effective values only. To emulate the experimental setup, no boundary conditions were prescribed to the model. Block Lanczos method was used to extract vibration modes and frequencies and to calculate the first flexural eigenfrequency of each sample.

2.8 | FE simulations of 3PB

In case of 3PB test, both the elastic modulus and the coefficient of thermal expansion of each added layer could be extracted by a comparison of the FE solution with the experimentally measured values (slopes of the loading curves) obtained for each loading direction. Generally, a matrix of reaction forces of the specimen to the applied displacement load for given E and CTE was calculated in the expected range for both loading geometries (i.e., $\alpha_{add} \in <7.5, 13.5 > 10^{-6}/K$, $E_{add} \in <1, 250 > GPa$); this resulted in two surfaces representing the slopes of the loading curves for given material properties of the added layer. Those FEA results, compared with the experimentally obtained slopes, provided a unique combination of E and CTE estimated for each added layer. The procedure adopted is depicted schematically in Figure 4.

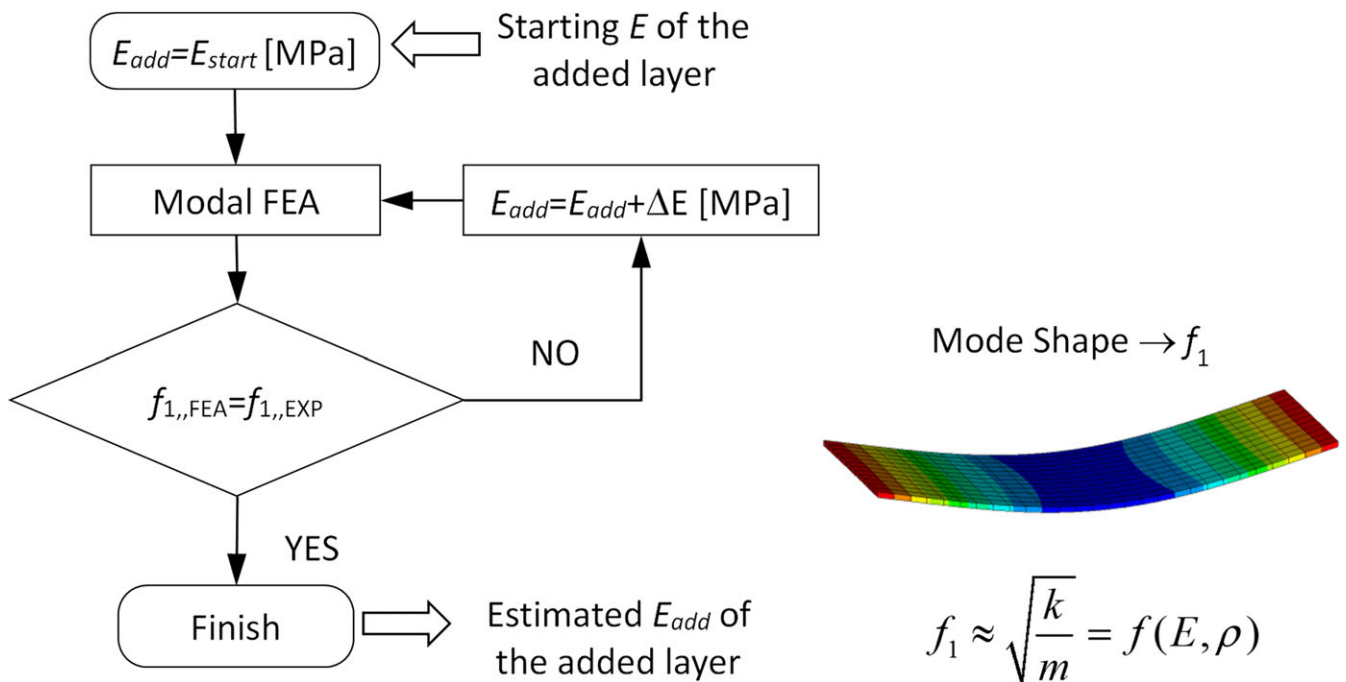


FIGURE 3 Scheme and FE model of the iterative FE simulation procedure to estimate elastic modulus of added layer by IET test

$$\begin{cases} F_{r,FEM,side1}(\alpha_{add}, E_{add}) - F_{r,FEM,side1} = 0 \\ F_{r,FEM,side2}(\alpha_{add}, E_{add}) - F_{r,FEM,side2} = 0 \end{cases}$$



$$\alpha_{add}, E_{add}$$

$$F_{r,FEM}(\alpha_{add}, E_{add}) : \text{calculated by FEA}$$

$$F_{r,EXP} : \text{measured experimentally}$$

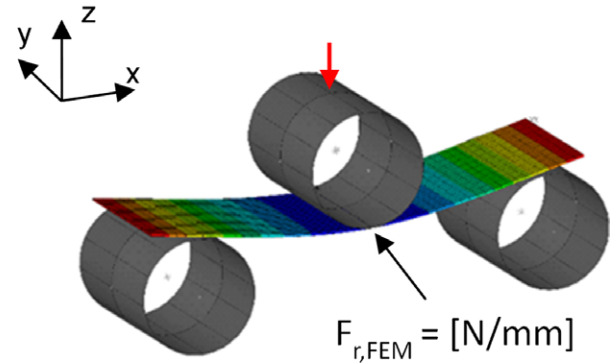


FIGURE 4 Scheme of the calculation of both CTE and elastic modulus of added layer from the 3PB test and example of the FE model

Since the deflection of the specimens during the 3PB test was large and the rotations of the mid-surface normal higher than 10° , the Kirchhoff hypothesis³⁴ was no longer valid. Hence, nonlinear solutions and large deformations had to be considered in FEA. Real contacts between cylindrical supports and samples were considered—see Figure 4—and the specimens were modeled as multi-layered structures with intrinsic residual stresses, except for the electrolyte (SOC0). To do that a temperature gradient ΔT of 1250°C was applied prior to the 3PB simulation, in order to simulate the cooling down from sintering temperature to room temperature. With the addition of layers (SOC1-SOC3), the CTE mismatch gives rise to residual stresses that are responsible, together with nonsymmetric design, for discrepancies in the deflections according to the tested side (i.e., which outer layer is in tension or compression). Poisson's ratios used for the layers were taken from literature^{23,35-37} and are summarized in Table 2, together with thicknesses and densities of individual layers.

All the numerical models were programmed using the APDL language in SW ANSYS 16.2. Quadratic shell elements SHELL281 of $200\ \mu\text{m}$ with multilayer option were chosen for the mesh in order to reduce computation costs.

3 | RESULTS

3.1 | Impulse excitation technique

The values of natural frequencies and derived elastic constants and Poisson's ratios obtained through the IET are summarized in Table 3 and shown graphically in Figure 5. In the graph, an average value with standard deviation for

each material type (SOC0-SOC3) is plotted. The deviation for each sample is relatively low, indicating the high reproducibility of the measurement. It was observed that the determined natural frequencies are independent on the side where the mechanical impulse excitation was applied. A continuous drop in the value of calculated elastic constants was observed since the adding of the very first GDC layer. For the SOC0 specimen, which corresponds to the monolithic 3YSZ ceramic, E and G have an average value of 202 GPa and 80 GPa, respectively; this result is in good agreement with the literature data for similar materials.³⁸⁻⁴¹ With the addition of the diffusion barrier layer (SOC1), the measured moduli drop significantly to approximately 80 % of the initial values (SOC0). When the fuel electrode is also added (SOC2) E and G decrease to 50 %, followed by a significant drop to 20 % of the electrolyte value in the presence of the LSCF air electrode layer (SOC3).

3.2 | Flexural test

The values of elastic modulus calculated from flexural tests are summarized in Table 3 and shown in Figure 6. Contrary to the results of IET, the flexural tests revealed a dependence on the loading orientation (i.e., which layer is in tension or compression); therefore Figure 6 shows results for both orientations. As for the values given by the IET, a continuous decrease in the elastic modulus was observed with the addition of layers to the electrolyte. For the electrolyte, E has an average value of 204 GPa, independently on the tested side; this result is in good agreement with the one obtained through the resonance method and the literature data.⁴²⁻⁴⁴ The measured elastic modulus

TABLE 2 Layer properties considered in the simulation

Layer	Material	Thickness [μm]	Density [g/cm ³]	ν [-]
Electrolyte	3YSZ	94	6.05	0.27
Barrier	GDC	6	4.02	0.26
Fuel electrode	NiO	24	5.97	0.25
Air electrode	LSCF	50	2.36	0.30

for the sample composed of the electrolyte and the thin GDC barrier layer (SOC1) slightly drops to 203 GPa and 193 GPa depending on the side in tension. A significant decrease in approximately 45% was detected for SOC2 on both tested sides. An even higher reduction was measured when the LSCF air electrode layer was also added (SOC3); in this case, the Young's modulus underwent a 77% drop when the fuel electrode was in tension and an even bigger decrease with the air electrode in tension (80%).

3.3 | Tensile test

The results calculated from the tensile tests are also presented in Table 3. The agreement between the E modulus obtained for the single electrolyte (SOC0) through the tensile test and the one measured by IET and three-point bending (and consequently the one reported in the literature), proves that the DIC based elongation measurement provides sufficiently accurate results. However, the elastic modulus obtained by tensile loading is the only one determined in accordance with the physical meaning of Young's modulus. This is the reason why the calculated values differ significantly from the ones obtained through the other methods as shown in Table 3. As an example, SOC3 Young's modulus in tension is 110 GPa while the one determined by IET or 3PB resides in the 40 to 45 GPa interval. To explain such differences a numerical analysis was necessary.

TABLE 3 E modulus, G modulus, Poisson's ratios and natural frequencies from IET, E modulus from 3PB and tensile tests. Standard deviations in brackets

	f_f [Hz]	f_t [Hz]	E_{IET}^a [GPa]	G_{IET}^a [GPa]	ν_{IET}^a [-]	$E_{3PB}^{b,c}$ [GPa]	$E_{3PB}^{d,c}$ [GPa]	$E_{tensile}$ [GPa]
SOC0	3227 (32)	4803 (14)	202.5 (1.9)	80.2 (0.5)	0.26 (0.01)	204.4 (1.2)	204.4 (1.2)	202.9 (3.2)
SOC1	3367 (62)	5031 (46)	166.4 (2.1)	66.4 (0.7)	0.25 (0.01)	192.8 (2.5)	203.2 (1.2)	195.7 (3.8)
SOC2	3324 (41)	5193 (40)	102.0 (1.6)	41.7 (1.1)	0.23 (0.02)	108.3 (1.7)	113.2 (0.5)	155.4 (4.5)
SOC3	3264 (51)	5082 (60)	40.8 (1.0)	16.4 (0.1)	0.23 (0.03)	46.3 (0.2)	41.2 (0.4)	110.4 (4.0)

^acalculated according to ASTM E1875-08 standard for isotropic materials.

^borientation fuel Electrode in tension.

^ccalculated according to EN 843-2 standard for monolithic ceramics.

^dorientation air Electrode in tension.

3.4 | FEA of IET and flexural test

The reverse iterative modal analysis allowed the determination of elastic properties of each added layer at the moment when the eigenfrequency calculated by FEA matched the one obtained experimentally for a given layered structure. The numerical simulation of the flexural test was based on the adjustment of the stiffness of each added layer to achieve the same overall stiffness obtained in the experiments. In this case, the nonsymmetrical layout of the samples, allowed the estimation of CTE values of each added layer, beside elastic modulus. Results from FEA for individual layers of the MEA layered structure are summarized in Table 4. In the table are also listed the results obtained by the application of the rule of mixture to the experimental data of the tensile test.

4 | DISCUSSION

The elastic moduli of the samples determined by different experimental techniques and listed in Table 3 can be divided into two groups according to the loading direction, i.e., out of plane (flexural) or in plane (tensile).

Regarding the 3YSZ electrolyte (SOC0), there is a very good agreement between the values obtained through all experimental techniques and also FEA due to isotropic nature of this layer. Whereas, with the increasing number of layers of the samples, the magnitude of Young's modulus determined by the tensile tests is significantly higher than the one determined by the resonance method and three-point bending (see Figure 7). The discrepancies between the methods show the complexity of mechanical behavior of the multi-layered nonsymmetrically arranged structure. The interactions between individual layers cannot be gathered by a single test technique. Moreover, due to the small sample thickness, it is not possible to meet all the requirements for the test standards (e.g., small deflections in 3PB test) and the resulting values have to be interpreted with caution. Therefore, we cannot speak about elastic

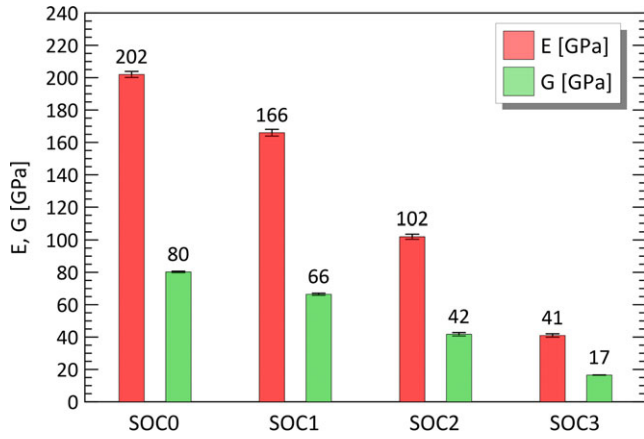


FIGURE 5 Elastic constants by a resonance method. Average bars with scatter

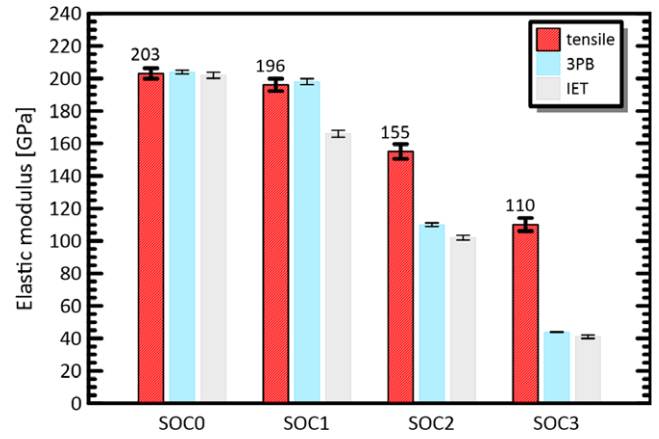


FIGURE 7 Average elastic modulus from tensile, flexural (3PB) and resonance tests (IET)

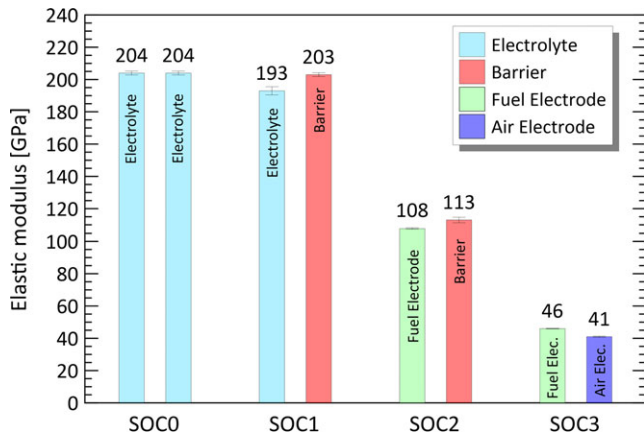


FIGURE 6 Average elastic modulus obtained through three-point bending test. The name of each column refers to the layer which is on the side in tension during the 3PB test

TABLE 4 E and CTE derived via FEA and RoM from IET, flexural (3PB), and tensile tests data

Layer	Material	E_{IET}^{FEA} [GPa]	E_{3PB}^{FEA} [GPa]	$E_{tensile}^{hboxRoM}$ [GPa]	CTE_{3PB}^{FEA} [$10^{-6}/K$]
Electrolyte	3YSZ	204	203	203	10.3
Barrier	GDC	70	120	102	10.7
Fuel Electrode	NiO	50	12	29	10.0
Air Electrode	LSCF	30	8	3	12.5

(Young's) modulus in its physical meaning, yet it would be more appropriate to refer to it as flexural stiffness in given direction. Nevertheless, the obtained results demonstrate the mechanical response of the material under a given loading configuration and are useful for practical

applications. In fact, bending and buckling are the main loading modes that the MEA undergoes during the service in a SOC stack. Hence, it is of high relevance to investigate the response of the MEA to flexural loadings.

In the case of 3PB tests, the determined elastic modulus of the MEA is acceptable in describing the overall flexural stiffness for a given orientation. This value is comparable to the one determined from IET tests since the same (flexural) loading is applied. Even if we cannot derive the effective elastic modulus, the natural frequencies determined by IET and the deflections measured by 3PB for a given material type were correctly determined. Therefore, these parameters were used for the determination of the elastic properties of each individual layer through FE simulations. The experimental results were considered as target response of the FE model and the properties of the individual layers were varied iteratively until the response of the model met the one measured experimentally (as shown in Figures 3 and 4). In this iterative process the properties of only one added layer at a time were changed. Once the properties of the added layer were determined, they were considered as fixed and used for assessing the properties of the subsequent added layer.

This process was demanding and not straightforward because of some complications. Firstly, the SOC laminate structure under investigation could not be homogenized, due to the nonsymmetrical and multi-material thin layered structure. Secondly, its substitution by an orthotropic continuum was not possible either because of the differences in the stiffness observed during the flexural tests, determined by the side in tension. Finally, the uncertainties given by the determination of the samples geometry (i.e., mainly the layer thicknesses) affected results significantly and had to be minimized by meticulous measurements.

The FEA of IET and 3PB led to the elastic characteristics of individual layers summarized in Table 4. The

TABLE 5 Comparison of E moduli obtained experimentally by tensile test and by rule of mixtures applied to IET and 3PB analytical data

	$E_{\text{tensile}}^{\text{Exp}}$ [GPa]	$E_{\text{IET}}^{\text{RoM}}$ [GPa]	$E_{\text{3PB}}^{\text{RoM}}$ [GPa]
SOC0	203	204	203
SOC1	196	195	197
SOC2	155	164	166
SOC3	110	125	119

comparison of data derived from different types of test, revealed significant differences between the applied loading conditions; however, the approach used in 3PB was able to provide also CTE values. The main reason of the difference can be seen in the high sensitivity of the simulation to the input data, especially the thickness of added layer, where just one micron change in the input can cause difference in tenth of percent in the output. One can also refer to Equation (1), where the thickness of the structure is in the third power; hence, a small change in this parameter has a significant influence on the derived Elastic modulus. The error analysis showed that this sensitivity is related to the thickness ratios (substrate to added layer). Therefore, even small input variation at beginning can end in several fold difference in the estimated elastic modulus at the last added layer. Once the elastic properties of individual layers were determined (see Table 4) the rule of mixture was applied to determine the overall elastic modulus. This was directly compared with the data obtained via tensile test, as shown in Table 5. The results for all the samples types are in good agreement when IET iterative modal FEA or 3PB based FEA are applied. An increase in the elastic response with the addition of layers to the electrolyte was detected in both cases, if compared with experimental data from tensile test. This phenomenon can be explained by the influence of co-sintering effects like development and consequent relaxation of residual stresses, interfacial bond effects or localized/gradient layers porosity which are not implemented to the FEA. Even though there is relatively good agreement in total stiffness calculated by rule of mixture the differences in elastic modulus of individual layers determined by both FEA is higher given by above noted uncertainties. Contrary to the sensitivity of elastic modulus the estimated CTE values are less sensitive and are rather connected with the absolute difference in the behavior between both loading directions (i.e., which outer layer is in tension or compression). Additionally when the reverse approach is applied to the experimental data from the tensile tests the similar values of elastic modulus are derived for individual layers as for numerical calculations (see Table 4). It has to be pointed

out again the strong influence of thicknesses measurement precision on the obtained results.

5 | CONCLUSIONS

The common approach for the measurement of elastic properties of layered materials is usually based on the evaluation of individual bulk materials. The main contribution of this work resides within the direct measurements of the elastic properties of layers when joined together, taking into account co-sintering effects and the possible effect of bi-material interfaces, which cannot be analyzed when individual bulk materials are investigated.

To obtain the overall stiffness of the multi-layered structure under investigation, three different loading approaches were applied. Those were accompanied by FEA, which allowed the derivation of characteristics for individual layers. The obtained results, helped to conclude the following:

1. The value of the elastic modulus (stiffness) decreases with the addition of layers to the electrolyte;
2. There is a good agreement between the results of the resonance method (IET) and the flexural test (3PB) due to the application of the same flexural loading mode;
3. All the techniques yielded to the same value of E for the electrolyte (SOC0); this value of approximately 203 GPa is also in agreement with those found in literature for the same material;
4. The significant discrepancy between results obtained through the flexural (out-of-plane) loading and the tensile (in-plane) one reveals that the MEA has to be treated as a nonsymmetrical laminate and the homogenization is not applicable;
5. The proposed FEA approaches can provide indicative values of elastic modulus for individual layers as well as CTE values when three-point bending experimental data are numerically analyzed for both orientations of the specimens;
6. The thicknesses of each added layer has a significant influence on the calculation of their elastic modulus.

ACKNOWLEDGMENTS

The research leading to these results has received funding from:

1. The European Union's Horizon 2020 research and innovation programme under the Marie Skłodowska-Curie project *CoACH (Advanced glasses, Composites And Ceramics for High growth Industries European Training Network)*, grant agreement No. 642557.

2. The Fuel Cells and Hydrogen 2 Joint Undertaking under grant agreement No 700300 (GrInHy, Green Industrial Hydrogen via reversible high-temperature electrolysis). This Joint Undertaking receives support from the European Union's Horizon 2020 research and innovation programme and Hydrogen Europe and N.ERGHY

ORCID

Alessia Masini  <http://orcid.org/0000-0002-6544-1857>

REFERENCES

- Lucia U. Overview on fuel cells. *Renew Sustain Energy Rev.* 2014;30:164-169.
- Ramadhani F, Hussain MA, Mokhlis H, et al. Optimization strategies for Solid Oxide Fuel Cell (SOFC) application: a literature survey. *Renew Sustain Energy Rev.* 2017;76:460-484.
- Dodds PE, Staffell I, Hawkes AD, et al. Hydrogen and fuel cell technologies for heating: a review. *Int J Hydrogen Energy.* 2015;40:2065-2083.
- Sharaf OZ, Orhan MF. An overview of fuel cell technology: fundamentals and applications. *Renew Sustain Energy Rev.* 2014;32:810-853.
- Laurencin J, Lefebvre-Joud F, Delette G. Impact of cell design and operating conditions on the performances of SOFC fuelled with methane. *J Power Sources.* 2008;177:355-368.
- Nakajo A, Mueller F, Brouwer J, et al. Progressive activation of degradation processes in solid oxide fuel cells stacks: part I: lifetime extension by optimisation of the operating conditions. *J Pow Sour.* 2012;216:449-463.
- Bodec T, Reytier M, Lhachemi D, et al. A new stack to validate technical solutions and numerical simulations. *Fuel Cells.* 2012;12:239-247.
- Sohal MS, Rashkeev SN, Glazoff MV, et al. *Modeling Degradation in Solid Oxide Electrolysis Cells.* Idaho Falls, ID: Idaho National Laboratory Report INL INL/EXT-09-15617; 2011.
- Fan P, Li G, Zeng Y, et al. Numerical study on thermal stresses of a planar solid oxide fuel cell. *Int J of Thermal Sci.* 2014;77:1-10.
- Peksen M. Numerical thermomechanical modelling of solid oxide fuel cells. *Prog Energy Combust Sci.* 2015;48:1-20.
- Nakajo A, Mueller F, Brouwer J, et al. Mechanical reliability and durability of SOFC stacks. Part I: modelling of the effect of operating conditions and design alternatives on the reliability. *Int J Hydrogen Energy.* 2012;37:9249-9268.
- Nakajo A, Mueller F, Brouwer J, et al. Mechanical reliability and durability of SOFC stacks. Part II: modelling of mechanical failures during ageing and cycling. *Int J Hydrogen Energy.* 2012;37:9269-9286.
- Frandsen HL, Ramos T, Faes A, et al. Optimization of the strength of SOFC anode supports. *J Eur Cer Soc.* 2012;32:1041-1052.
- Selçuk A, Atkinson A. Elastic properties of ceramic oxides used in solid oxide fuel cells (SOFC). *J Eur Cer Soc.* 1997;17:1523-1532.
- Atkinson A, Selçuk A. Mechanical behaviour of ceramic oxygen ion-conducting membranes. *Solid State Ionics.* 2000;134:59-66.
- Giraud S, Canel J. Young's modulus of some SOFCs materials as a function of temperature. *J Eur Cer Soc.* 2008;28:77-83.
- Kushi T, Sato K, Unemoto A, et al. Elastic modulus and internal friction of SOFC electrolytes at high temperatures under controlled atmospheres. *J Pow Sour.* 2011;196:7989-7993.
- Kushi T, Sato K, Unemoto A, et al. Investigation of High Temperature Elastic Modulus and Internal Friction of SOFC Electrolytes Using Resonance Method. *ECS Trans.* 2009;25:1673-1677.
- Fleischhauer F, Bermejo R, Danzer R, et al. High temperature mechanical properties of zirconia tapes used for electrolyte supported solid oxide fuel cells. *J Pow Sour.* 2015;273:237-243.
- Fleischhauer F, Bermejo R, Danzer R, et al. Strength of an electrolyte supported solid oxide fuel cell. *J Pow Sour.* 2015;297:158-167.
- Yavo N, Noiman D, Wachtel E, et al. Elastic moduli of pure and gadolinium doped ceria revisited: sound velocity measurements. *Scripta Mater.* 2016;123:86-89.
- Delette G, Laurencin J, Usseglio-Viretta F, et al. Thermo-elastic properties of SOFC/SOEC electrode materials determined from three-dimensional microstructural reconstructions. *Int J Hydrogen Energy.* 2013;38:12379-12391.
- Nakajo A, Kuebler J, Faes A, et al. Compilation of mechanical properties for the structural analysis of solid oxide fuel cell stacks. Constitutive materials of anode-supported cells. *Cer Int* 2012;38:3907-3927.
- Johnson J, Qu J. Effective modulus and coefficient of thermal expansion of Ni-YSZ porous cermets. *J Pow Sour.* 2008;181:85-92.
- Tabei SA, Sheidaei A, Baniassadi M, et al. Microstructure reconstruction and homogenization of porous Ni-YSZ composites for temperature dependent properties. *J Pow Sour.* 2013;235:74-80.
- Roebben G, Basu B, Vleugels J, et al. Transformation-induced damping behaviour of Y-TZP zirconia ceramics. *J Eur Cer Soc.* 2003;23:481-489.
- Bermejo R, Sanchez-Herencia AJ, Llanes L, et al. High-temperature mechanical behaviour of flaw tolerant alumina-zirconia multilayered ceramics. *Acta Mater.* 2007;55:4891-4901.
- Raj SV, Pawlik R, Loewenthal W. Young's moduli of cold and vacuum plasma sprayed metallic coatings. *Mater Sci Eng.* 2009;513-514:59-63.
- Roebben G, Bollen B, Brebels A, et al. Impulse excitation apparatus to measure resonant frequencies, elastic moduli, and internal friction at room and high temperature. *Rev Sci Instrum.* 2009;68:4511-4515.
- ASTM E1875-08 Standard Test Method for Dynamic Young's Modulus, Shear Modulus, and Poisson's Ratio by Sonic Resonance. West Conshohocken, PA: ASTM International; 2008.
- EN 843-2 Advanced technical ceramics - Monolithic ceramics. Mechanical properties at room temperature - Part 2: Determination of Young's modulus, shear modulus and Poisson's ratio. Brussels: European Committee for Standardization; 2006.
- Hild F, Roux S. Digital image correlation: from displacement measurement to identification of elastic properties - A review. *Strain.* 2006;42:69-80.
- Klemensø T, Lund E, Sørensen BF. Optimal shape of thin tensile test specimen. *J Am Cer Soc.* 2007;90:1827-1835.

34. Whitney JM. *Structural Analysis of Laminated Anisotropic Plates*. Lancaster, PA: Technomic Pub. Co; 1987;342.
35. Boccaccini DN, Sevecek O, Frandsen HL, et al. Investigation of the bonding strength and bonding mechanisms of SOFCs interconnector-electrode interfaces. *Mater Lett*. 2016;162:250-253.
36. Liu L, Kim GY, Chandra A. Modeling of thermal stresses and lifetime prediction of planar solid oxide fuel cell under thermal cycling conditions. *J Pow Sour*. 2010;195:2310-2318.
37. Boccaccini DN, Sevecek O, Frandsen HL, et al. Determination of the bonding strength in solid oxide fuel cells' interfaces by Schwickerath crack initiation test. *J Eur Cer Soc*. 2017;37:3565-3578.
38. Lange FF. Transformation toughening - Part 5 Effect of temperature and alloy on fracture toughness. *J Mat Sci*. 1982;17:255-263.
39. Winnubst AJA, Keizer K, Burggraaf AJ. Mechanical properties and fracture behaviour of ZrO₂-Y₂O₃ ceramics. *J Mat Sci*. 1983;18:1958-1966.
40. Pihlatie M, Kaiser A, Mogensen M. Mechanical properties of NiO/Ni-YSZ composites depending on temperature, porosity and redox cycling. *J Eur Cer Soc*. 2009;29:1657-1664.
41. Nawa M, Yamazaki K, Sekino T, et al. Microstructure and mechanical behaviour of 3Y-TZP/Mo nanocomposites possessing a novel interpenetrated intragranular microstructure. *J Mat Sci*. 1996;31:2849-2858.
42. Anandakumar G, Li N, Verma A, et al. Thermal stress and probability of failure analyses of functionally graded solid oxide fuel cells. *J Pow Sour*. 2010;195:6659-6670.
43. Bamba N, Choa YH, Sekino T, et al. Mechanical properties and microstructure for 3 mol % yttria doped zirconia/silicon carbide nanocomposites. *J Eur Cer Soc*. 2003;23:773-780.
44. Vaidya S, Kim JH. Continuum mechanics of solid oxide fuel cells using three-dimensional reconstructed microstructures. In: Gan YX, ed. *Chapter 4 in Continuum Mechanics - Progress in Fundamentals and Engineering Applications*. Rijeka: InTech; 2012;73-88.

How to cite this article: Masini A, Šiška F, Ševeček O, Chlup Z, Dlouhý I. Elastic properties of multi-layered ceramic systems for SOCs. *Int J Appl Ceram Technol*. 2017;00:1-10. <https://doi.org/10.1111/ijac.12801>